REVIEW OF SCIENTIFIC INSTRUMENTS **89**, 083702 (2018)

Monochromatic mammography using scanning multilayer X-ray mirrors

David L. Windt[a)]
Reflective X-ray Optics LLC, 425 Riverside Dr., New York, New York 10025, USA

(Received 26 May 2018; accepted 21 July 2018; published online 16 August 2018)

A prototype system for breast imaging using monochromatic X-rays has been developed using a scanning multilayer X-ray mirror in combination with a conventional mammography tube and an imaging detector. The X-ray mirror produces a monochromatic fan beam tuned near 19 keV, with an energy bandpass of approximately 1.5 keV. Rotating the mirror about the tube's focal spot in synchronization with the X-ray generator and detector enables the acquisition of monochromatic X-ray images over large areas. The X-ray mirror also can be rotated completely out of the beam so that conventional polychromatic images can be acquired using a K-edge filter, facilitating direct comparison between the two modes of operation. The system was used to image synthetic, tissue-equivalent breast phantoms in order to experimentally quantify the improvements in image quality and dose that can be realized using monochromatic radiation. Nine custom phantoms spanning a range of thicknesses and glandular/adipose ratios, each containing both glandular- and calcification-equivalent features, were used to measure contrast and signal-difference-to-noise ratio (SDNR). Mean glandular dose (MGD) was computed from measured entrance exposure, and a figure-of-merit (FOM) was computed as FOM = $SDNR^2$/MGD in each case. Monochromatic MGD ranges from 0.606 to 0.134 of polychromatic MGD for images having comparable glandular SDNR, depending on breast thickness and glandularity; relative monochromatic dose decreases with increasing glandularity for all thicknesses. Monochromatic FOM values are higher than the corresponding polychromatic FOM values in all but one case. Additionally, the monochromatic contrast for glandular features is higher than the polychromatic contrast in all but one case as well. These results represent important steps toward the realization of clinically practical monochromatic X-ray breast imaging systems having lower dose and better image quality, including those for digital mammography, digital breast tomosynthesis, contrast-enhanced spectral mammography and other modalities, for safer, more accurate breast cancer detection, diagnosis and staging. *Published by AIP Publishing.* https://doi.org/10.1063/1.5041799

I. INTRODUCTION

X-ray mammography is the most widely used technique for breast imaging. Screening for breast cancer using digital mammography (DM) has reduced mortality rates significantly, but it suffers from imperfect sensitivity and specificity.[1] Digital breast tomosynthesis (DBT), where a quasi-3D representation of the breast is constructed from multiple DM images acquired over a limited range of projection angles,[2] has greatly reduced the challenges associated with overlapping structures in the breast in DM, and has led to significant clinical benefits.[3] Nevertheless, inaccuracies and other limitations in DM and DBT, partly due to achievable image quality (IQ) and allowable radiation dose, constrain the ability of radiologists to distinguish deadly from non-deadly cancers, and lead to overdiagnosis and overtreatment.

Mammography requires the use of relatively low energy X-rays for maximum contrast between adipose and non-adipose (both glandular and malignant) tissue.[4] Commercial DM and DBT systems utilize the broad spectrum of X-rays emitted from a conventional electron-impact X-ray tube. The X-ray spectrum is shaped, and thus optimized for a specific breast thickness and glandularity, by the choice of the tube anode material (typically Mo, Rh or W), by the choice of the tube voltage (typically set below about 35 kVp), and by the use of transmission filters such as Mo, Rh and others used to reduce the intensity of unwanted X-rays having energies above the K-edge of the filter material.[5,6] Even so, the emitted X-ray spectrum remains relatively broad, degrading performance due to beam hardening: low energy X-rays are predominantly absorbed by the tissue, increasing dose, while high energy X-rays pass through the tissue unattenuated, decreasing image contrast.[7]

Breast imaging using monochromatic X-rays promises lower dose and better image quality (IQ) relative to the conventional approach, performance benefits that have been established from both modeling[8] and experiments.[9–14] A clinical mammography system operating with monochromatic X-rays in the 15–50 keV energy range would lead to improved IQ and reduced dose for both DM and DBT; it would also enable improved performance in dual-energy contrast-enhanced spectral mammography (CESM),[15] a technique that uses an iodine contrast agent and combines images acquired at energies above and below the iodine K-edge to derive both a morphological breast image and a functional (iodine) image highlighting vascularity to identify tumors.[16] The performance improvements resulting from the use of monochromatic radiation in these imaging modalities could potentially lead to better identification of deadly cancers, reductions in overdiagnosis and overtreatment, and other clinical benefits. Monochromatic

a)davidwindt@gmail.com. Tel.: 347-850-2212.

X-ray imaging may also yield clinical benefits in contrast-enhanced DBT, breast computed tomography, dual-energy bone density scanners, small animal CT and other imaging applications as well.

Experimental breast imaging using monochromatic X-rays has been conducted using specialized light sources,[9,10] including promising clinical research based on phase-contrast imaging techniques using synchrotron radiation.[11] Monochromatic breast imaging research has also been conducted using X-rays that are generated by conventional electron-impact X-ray tubes and that are either diffracted by crystal optics,[12] transmitted by polycapillary optics[13] or reflected by multilayer X-ray mirrors.[14] The long-term objective of the present research is to develop an affordable monochromatic X-ray breast imaging system that could be widely implemented in clinical practice, using multilayer X-ray mirrors and standard medical X-ray tubes.

A prototype monochromatic X-ray imaging test-stand has been constructed using a scanning multilayer X-ray mirror in conjunction with a standard mammography tube and a fixed imaging detector arranged in a conventional mammographic configuration. The test-stand also can be operated with conventional K-edge filters, without the multilayer mirror, for polychromatic imaging, facilitating direct comparison of dose and IQ between the two modes of operation, using a common tube and detector. In order to quantify the relative performance benefits that can be realized using monochromatic X-rays so generated, the test-stand was used to conduct a preliminary systematic investigation of dose and IQ as a function of breast thickness and glandularity, using an array of custom-made breast phantoms, for both monochromatic (19 keV) and polychromatic X-rays.

II. MATERIALS AND METHODS

A. Imaging test-stand

The prototype imaging test-stand is shown schematically in Fig. 1: the configuration used for monochromatic imaging is shown in Fig. 1(a) and that used for conventional polychromatic imaging, with the X-ray mirror removed from the beam, is shown in Fig. 1(b). The system uses a W-anode mammography tube (Varian model M-113T and B-110 housing) having both 0.1 mm and 0.3 mm focal spots, and 0.63 mm of intrinsic Be filtration. The tube is controlled by an X-ray generator that can be operated from 20 to 49 kVp (Sedecal model SHF330SC). Transmission filters can be inserted in a holder positioned just below the exit port of the tube. Images are obtained using a CMOS mammography detector (Dexela

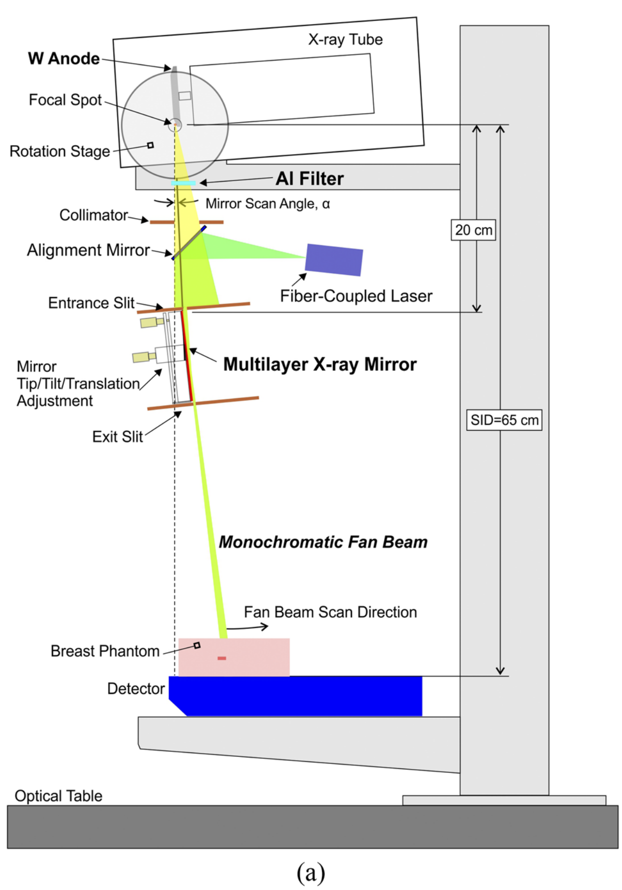

FIG. 1. Schematic diagram of the imaging test-stand developed for the investigation of monochromatic X-ray breast imaging. (a) The configuration used for monochromatic imaging utilizes a multilayer X-ray mirror and 0.2 mm of Al filtration to produce a quasi-monochromatic fan beam tuned near 19 keV that can be rotated (scanned) about the focal spot during exposure for large-area imaging. Entrance and exit slits located on either side of the mirror ensure that only X-rays reflected by the mirror reach the image plane. (b) For polychromatic imaging, the Al filter is replaced with a 0.05 mm-thick Rh filter, and the scanning mirror is rotated out of the cone beam. A high-precision optical alignment system, comprising a fiber-coupled green laser and an Al-coated glass mirror (0.21 mm thickness) oriented at ~45° relative to the cone beam, was developed for alignment of the X-ray mirror.

model 2923M) having a 150 μm-thick CsI scintillator and a 3888 × 3872 array of 74.8 μm-wide pixels. A brass collimator is used to define the size of the beam: at the image plane, located at a source-to-image (SID) distance of 65 cm from the tube focal spot, the illuminated area measures ∼16 cm × ∼22 cm. The components are mounted rigidly on an optical table, in a vertical orientation, although the technology could be made to work in any orientation (and/or with other SID values), as would be required for oblique views or for DBT. An ionization chamber and high-purity Al attenuators for the measurement of dose and half-value layer (HVL),[7] as described in Sec. II D, and an energy-sensitive CdTe detector for spectral measurements,[17] described in Sec. II E, can be easily installed.

Flat X-ray multilayer mirrors can be mounted between the tube and the detector to generate monochromatic radiation. An X-ray multilayer coating consists of a stack of nm-scale bilayers of two materials having a large difference in their optical properties at the target X-ray energies. The multilayer coatings work by optical interference,[18] with the condition for constructive interference given (approximately) by Bragg's law: $n\lambda = 2d \sin\theta$, where n = 1, 2, … is the Bragg order, λ is the X-ray wavelength, d is the multilayer period, i.e., the thickness of one bilayer in the film stack, and θ is the grazing incidence angle. The energy response of a mirror operating at a given incidence angle thus can be controlled by adjusting the multilayer period during film deposition.

A schematic diagram of the multilayer mirror used for this investigation is shown in Fig. 2. The edge of the 100 mm-long mirror closest to the tube is positioned 20 cm from the tube focal spot when mounted in the test-stand [Fig. 1(a)]. The intersection of the cone beam emitted by the tube with the plane mirror results in a linear variation in the grazing incidence angle of X-rays relative to the mirror surface along the length of the mirror, as shown in Fig. 2: the mirror is aligned for an incidence angle of $\theta_{max} = 0.6°$ at the edge of the mirror closest to the tube, and $\theta_{min} = 0.4°$ at the far edge of the mirror. In order to ensure that the entire mirror surface reflects the same X-ray wavelength, the condition for constructive interference must be satisfied at each location on the mirror surface, taking into account the variation in incidence angle along the length of the mirror (i.e., Fig. 2), as well as the (much smaller) variation in incidence angle along the width of the mirror due to the beam divergence in that direction as well. As a result of these variations in incidence angle, the multilayer period must vary correspondingly over the surface of the mirror, in accord with Bragg's law.

The mirror is mounted to a multi-axis positioner used for precise mirror alignment relative to the focal spot. A brass plate with a machined entrance slit is fixed to the mount in front of the mirror, and a second plate with an exit slit is positioned just after the mirror [Fig. 1(a)] to ensure that only X-rays reflected by the mirror surface reach the detector. With a 100 × 100 mm^2 mirror oriented relative to the X-ray cone-beam following the geometry just described, the reflected X-rays form a monochromatic fan beam measuring 2.3 mm in width × 22 cm in length at the image plane (i.e., for a SID of 65 cm).

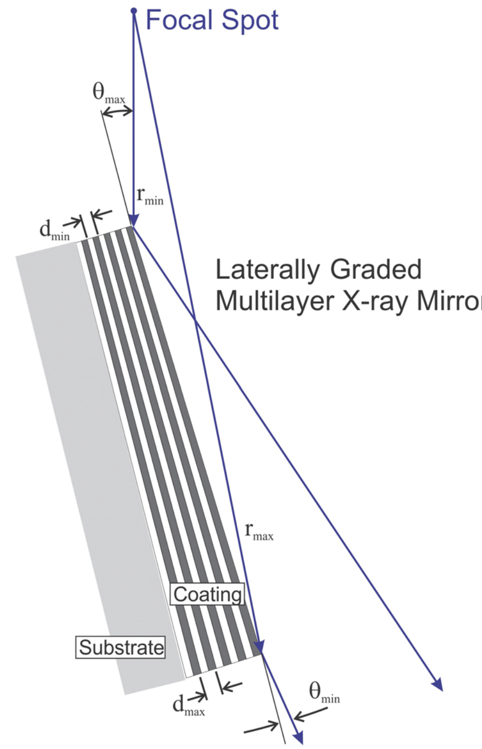

FIG. 2. Schematic diagram of a laterally graded multilayer X-ray mirror illuminated by radiation emitted from a point source, e.g., from a conventional mammography X-ray tube. The aspect ratio in this diagram is greatly distorted for clarity. Unlike a crystal monochromator, the multilayer coating, which is deposited on a thin flat substrate, can be fabricated with a precise lateral gradation in multilayer period so that the entire mirror surface reflects only over a narrow range of X-ray energies, in accordance with Bragg's law.

Large area illumination can be achieved by scanning the mirror during the exposure, with the tube, tissue (phantom) and detector fixed in place. The test-stand includes such a mirror-scanning mechanism, specifically designed to maintain precise alignment of the mirror (and the entrance and exit slits) relative to the focal spot during the scan.[19] The scan velocity is computer-controlled so as to match the tube exposure time and the desired angular scan length. The position of the scanner's rotation axis relative to the X-ray tube is adjusted via two orthogonal linear translation stages [not shown in Fig. 1(a), but explained in detail in Ref. 19] so that the rotation axis can be made to be coincident with the X-ray tube's focal spot, thereby maintaining precise mirror alignment and thus constant spectral response, at any scan angle α. The mirror scan is driven by a motorized rotation stage (Newport model RV-120PP-F) having a resolution of 0.002°, controlled by a programmable motion controller (Newport model XPS-Q8). Custom microprocessor-based electronics were developed (RPM Associates, Boulder, CO) to precisely synchronize the tube output with the detector readout cycle and, in the case of monochromatic exposures using the multilayer mirror, with the mirror scan motion. Also incorporated into the test-stand is an optical alignment system, utilizing a fiber-coupled green laser and a 0.21 mm-thick Al-coated glass mirror, which is used to facilitate mirror alignment.[20] The alignment system is analogous to the visible-light registration systems that are incorporated into conventional mammography systems, but with higher precision for accurate mirror alignment at small graze angles.

B. Multilayer x-ray mirror

For this research a multilayer coating comprising 40 bilayers of silicon-carbide (SiC) and tungsten (W) was deposited onto a 100 × 100 × 0.6 mm^3 polished Si substrate, using magnetron sputtering. The multilayer deposition system and the methods used to produce the coating were developed previously.[18,21] A specific lateral gradation in the multilayer period across the mirror surface is achieved through the use of baffles during film deposition.[22] An X-ray energy of ∼18.5 keV was selected for the preliminary imaging work described below, and so the multilayer period was designed to vary nearly linearly from d ≈ 3.4 nm to d ≈ 5.5 nm along the center line of the mirror, in order to match the range of incidence angles present when the mirror is mounted in the test-stand and illuminated by the cone beam of X-rays (Fig. 2). The thicknesses of the SiC and W layers in each bilayer were set equal, even though higher reflectance in the 1st Bragg order can be achieved using thinner W layers; this was done specifically to suppress 2nd order Bragg reflections that can occur when the tube is operated at sufficiently high voltage.

The X-ray reflectance of the mirror was measured using a custom-built hard X-ray reflectometer system.[23] The measurement geometry is shown in Fig. 3. The plane of incidence is horizontal, while the direction of the multilayer lateral gradation on the substrate is vertical; the reflectance as a function of energy can be measured at different positions on the mirror by translation of the mirror vertically (using a motorized translation stage). Reflectance measurements were made every 10 mm along the length of the mirror, in addition to two measurements made at positions located 3 mm from each edge of the mirror, for a total of 11 measurement locations along the center line of the mirror. The measurement locations thus range from r = 203 mm to r = 297 mm, where r is defined as the distance from a point on the mirror surface to the focal spot of the tube when the mirror is mounted in the test-stand scanner, as indicated in Fig. 3. A low-divergence X-ray beam measuring 40 μm-wide × 1 mm-high was used for the reflectance measurements, and the incidence angle θ was adjusted at each measurement position on the mirror surface so as to match the incidence angle at that same position when the mirror is used with the cone-beam emitted by the mammography tube in the test-stand, to within ±0.005°.

The resulting ensemble of measured reflectance-vs.-X-ray-energy curves is shown in Fig. 4, along with the "average" reflectance curve computed from the ensemble. The peak reflectance of the mirror ranges from ∼65% to ∼75%, depending on position/angle, with an average value over the surface of 68%. The surface-averaged curve is centered near 18.5 keV, as designed, with a bandpass of ∼1.3 keV full-width-half-maximum (FWHM).

Higher order radiation from the multilayer coating must be suppressed in order to mitigate unwanted high-energy X-rays in the monochromatic beam used for imaging. The reflectance at the 2nd order Bragg peak near 35 keV for the mirror used here was measured to be less than 0.5% at all 11 positions sampled on the mirror surface. Figure 5 shows a semi-log plot of an example reflectance curve, in this case measured at the center of the mirror (r = 250 mm), where the incidence angle was set to θ = 0.481°. The measured reflectance (red, online version only) agrees well with the calculated reflectance (blue, online version only), computed using the IMD program,[24] assuming 0.3 nm-wide interface widths. In this example, the 2nd order reflectance is less than 0.2%. The 3rd order reflectance is nearly 3%, but is centered near 51.4 keV, so no radiation can be reflected in 3rd order even when used with the mammography tube operating at maximum voltage, i.e., 49 kVp; similar results were obtained at other locations on the mirror surface.

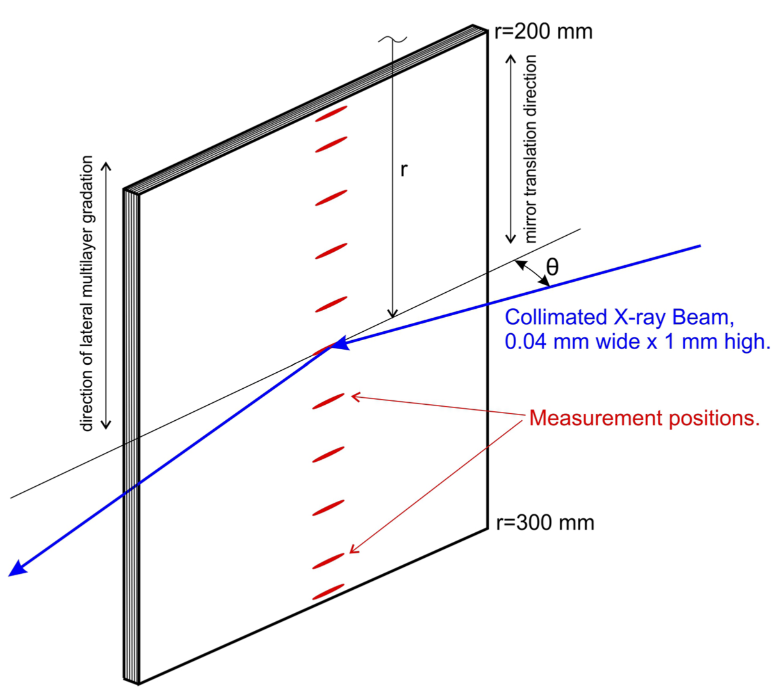

FIG. 3. Geometry used to measure reflectance-vs-energy as a function of position, r, at 11 locations on the laterally graded SiC/W multilayer X-ray mirror used for this research. The incidence angle θ was adjusted at each measurement position so as to match the incidence angle at that same position when the mirror is used with the cone-beam emitted by the mammography tube in the test-stand.

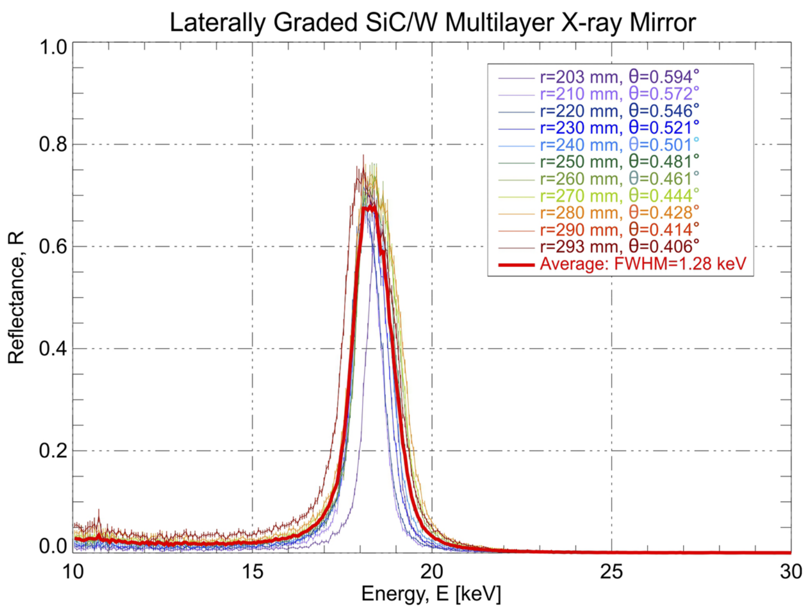

FIG. 4. Reflectance-vs-energy of the laterally graded SiC/W multilayer X-ray mirror used for this research, measured at the positions and incidence angles (r, θ) indicated in the legend. (The 100 mm-long mirror extends from r = 200 to r = 300 mm, as shown in Fig. 3.) The surface-averaged reflectance curve has a peak reflectance of ~0.68 and a bandpass of 1.3 keV FWHM (i.e., as measured with the low-divergence beam used in the hard X-ray reflectometer).

C. Breast phantoms

The methodology for the measurement of IQ adopted for this work was developed by Williams *et al.*,[25] and uses synthetic, tissue-equivalent breast phantoms containing embedded features that simulate various types of lesions, in order to compute statistical image properties specific to those lesions. Custom phantoms (CIRS, Inc., Norfolk, VA), identical to those used (and more fully described) in Ref. 25, are assembled from 10 cm × 12.5 cm plates of various thickness and glandularity. Plates comprising 30%, 50% and 70% glandularity were used to construct phantoms of 3, 5 and 7 cm thickness; thus a total of 9 different phantoms were used for IQ measurements in this investigation. In each case, the phantom assembly included two outer 5 mm-thick plates of 100% adipose-equivalent material, to simulate skin. The central plate in all cases was 2 cm thick, was also constructed of either 30%, 50% or 70% glandularity materials, and contained the embedded features. For this preliminary investigation, image contrast and SDNR were computed for two specific features: a 10 mm-thick square step (1 cm × 1 cm) of 100% glandular-equivalent material and a 0.3 mm-thick square step (also 1 cm × 1 cm) of calcification-equivalent material. The breast phantoms were placed directly on the surface of the imaging detector during image acquisition, with the two steps used for image quality computations located approximately 5 cm from the chest wall position.

D. Dose measurements

Entrance exposure, used to compute dose, was measured using a calibrated 15 cm^3 mammographic ionization chamber (Fluke model 96035B) and exposure meter (Fluke model 35050AT). The ionization chamber was mounted in the test-stand at the same distance from the focal spot as the surface of a 3 cm-thick breast phantom when placed on the imaging detector, and the center of the ionization chamber was coincident with the 0.3 mm-thick calcification step. The distance-adjusted entrance exposure (i.e., in units of mRad) for thicker phantoms was computed by scaling the measured normalized entrance exposure (i.e., in units of mrad/mA s) for the 3 cm-thick phantom by the ratio of the squares of the source-to-object distances

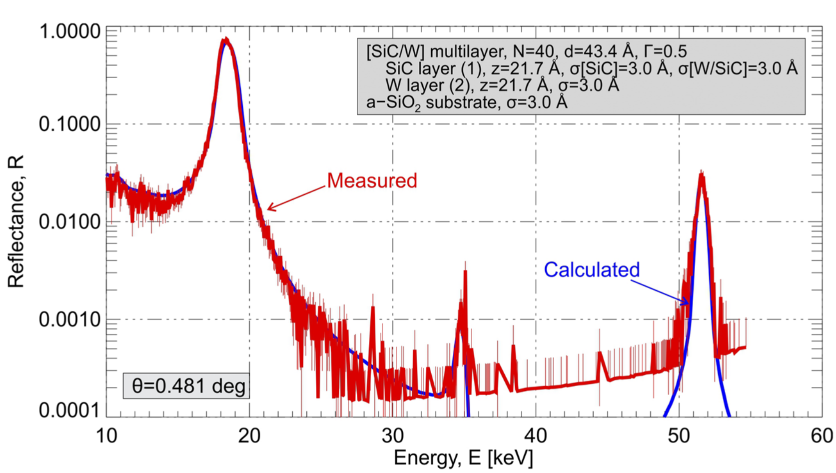

FIG. 5. Measured (red, online version only) reflectance at the center of the multilayer X-ray mirror used for this research. The coating was designed to have nearly equal thicknesses of W and SiC layers throughout the film stack, in order to suppress the 2nd-order Bragg peak, at the expense of peak reflectance in 1st order. The measured reflectance agrees well with the reflectance calculated using the IMD program (blue, online version only), assuming 0.3 nm-thick interface widths in the multilayer stack.

for the 5 and 7 cm phantoms, and by the actual current-time product (mA s) used to acquire a given image.

For the case of polychromatic X-rays, where a 50 μm-thick Rh filter was used, normalized entrance exposure was determined for tube voltages ranging from 20 to 34 kVp, in 2 kVp steps. Mean glandular dose (MGD) was computed from the measured entrance exposure using Boone's tabulated normalized glandular dose (DgN) data for W/Rh based on Monte Carlo calculations,[26] interpolating between the published HVL and glandularity values. A set of ultrahigh-purity 0.1 mm-thick Al attenuators (Fluke model 07-434) was used to determine the HVL value at each tube voltage.

For the case of monochromatic X-rays produced using the multilayer mirror, 200 μm of Al filtration was used in place of the Rh filter to preferentially attenuate low-energy X-rays (i.e., E < ∼10 keV) that are reflected from the multilayer X-ray mirror by total external reflection. Normalized entrance exposure [mRad/mA s] was computed as the entrance exposure [mRad], measured while the monochromatic fan beam was scanned over an angular range of $\Delta\alpha = 6°$, divided by the mA s value used for the measurement; however, the mA s value was first scaled by the sum of the angle subtended by the 3.96-cm-OD ionization chamber (3.64°) and the angular width of the fan beam (0.2°), divided by the scan range ($\Delta\alpha = 6°$) used during the exposure measurement, a quantity that is proportional to the fraction of the exposure time during which the ionization chamber was actually illuminated. MGD for monochromatic radiation (i.e., E = 19 keV) was computed from the distance- and current-time-product-adjusted entrance exposure using Boone's parameterized DgN data for monochromatic radiation,[27] also determined from Monte Carlo calculations, again interpolating between the published glandularity values for each breast phantom.

E. X-ray spectra measurements

X-ray spectra were acquired using an energy-sensitive CdTe detector system (Amptek model XR-100T-CdTe, with PX5 electronics). The energy scale of the detector system was calibrated using the prominent 13.95 and 59.54 keV lines from an ^{241}Am source. A 1 mm-thick W disc with a 25 μm-diameter pinhole was mounted a few cm above the entrance aperture of the detector to prevent saturation during exposure with the mammography X-ray tube. The CdTe detector was mounted on a tip-tilt stage, and the orientation of the detector and pinhole relative to the X-ray beam was systematically adjusted to maximize throughput for each measurement. Polychromatic spectra obtained at several tube voltages, using a current-time product of 100 mA s in all cases, are shown in Fig. 6, along with a monochromatic spectrum obtained using the SiC/W multilayer X-ray mirror, a tube voltage of 49 kVp and 320 mA s. (Note that the pinhole was re-aligned for the monochromatic spectrum acquisition, so the relative intensity of the monochromatic spectrum to the polychromatic spectra cannot be determined from Fig. 6.) The bandpass of the mirror in the cone-beam geometry is approximately 1.5 keV FWHM, which is slightly larger than that measured using a low-divergence pencil beam in the hard X-ray reflectometer (Sec. II B). The difference in bandpass is due to the larger divergence in the cone-beam geometry, stemming from the 0.1 mm spot size and relatively close proximity of the mirror to the source (i.e., r = 200 mm), which results in a wider range of X-ray energies that satisfy the Bragg condition for constructive interference at each point on the mirror surface.

The CdTe detector is also used during mirror alignment to ensure good spectral uniformity (and thus acceptable mirror alignment) within the entire 22 cm-long by 2.3 mm-wide monochromatic fan beam. Spectral uniformity across the width of the fan beam was determined by recording spectra at several locations within the beam, with the detector and pinhole fixed for each measurement, and the mirror scanned in $\Delta\alpha = 0.1°$ steps. Spectral uniformity in the perpendicular direction was determined by manually repositioning and realigning the detector at several points along the length of the fan beam. Additionally, the detector is used to accurately position the

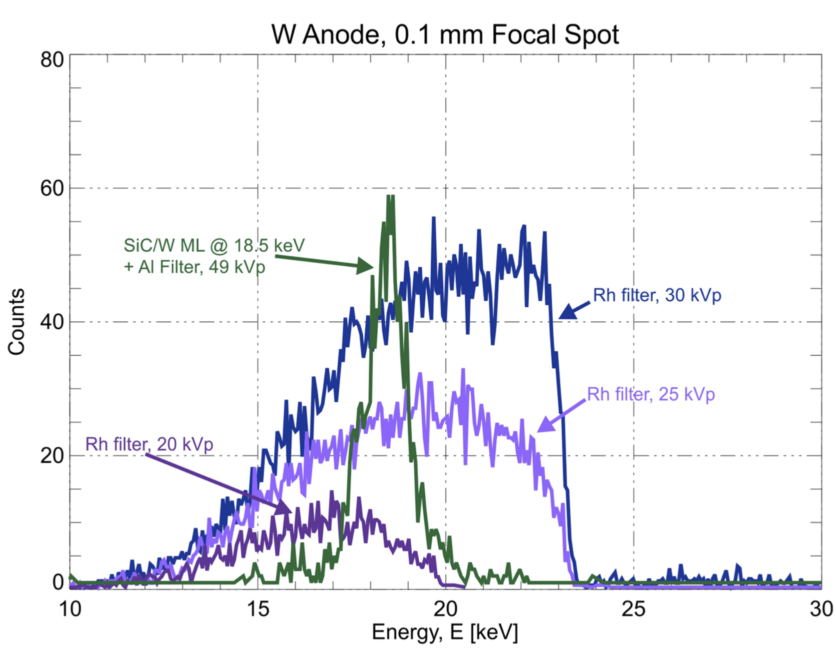

FIG. 6. X-ray spectra obtained using the W anode and a 0.05 mm-thick Rh filter at tube voltages of 20, 25 and 30 kVp, and a current-time product of 100 mA s, as well as the spectrum obtained using the multilayer X-ray mirror and 0.2 mm of Al filtration (with the tube at 49 kVp, 320 mA s, and a different pinhole alignment). The spectrum of X-rays reflected by the mirror has an energy bandpass of ∼1.5 keV FWHM when illuminated with the cone-beam of X-rays emanating from the 0.1 mm focal spot.

mirror scan axis to be coincident with the tube's focal spot, to ensure that the spectrum does not vary as the mirror is scanned. An iterative procedure is followed: the spectrum near the image plane is sampled at various points over the scan range, with the detector manually repositioned and realigned at each sampling location; the scan axis position is adjusted until spectral variations over the scan range are eliminated.

F. Image acquisition

Custom software running on a Linux-based computer was used for instrument control, data acquisition and analysis. Both dark-field (offset) and flat-field (gain) image corrections were performed on all acquired phantom images, following the conventional methodology in which the corrected image data $C(x, y)$ are derived from the raw image data $I(x, y)$ using

$$C(x,y) = \bar{g}\,\frac{I_{t_2}(x,y) - B_{t_2}(x,y)}{G_{t_1}(x,y) - B_{t_1}(x,y)}, \qquad (1)$$

where $B(x, y)$ is the averaged dark-field image, $G(x, y)$ is the averaged flat-field image, and $\bar{g}$ is the mean pixel value of $G(x, y)$. The subscripts t_1 and t_2 indicate that different exposure times may be used for acquisition of the flat-field and raw image data.[28]

Dark-field images were acquired for exposure times ranging from 50 to 10 000 ms; 10 dark images were median-combined to compute an average dark-field image for each exposure time. For polychromatic imaging, flat-field images were acquired at tube voltages in the range 20–34 kVp, in 2 kVp increments. The exposure time was adjusted for each tube voltage so that the maximum pixel value detected was in the range 12 000–15 000 (i.e., sufficiently below the maximum allowable value of 16 383, to avoid pixel saturation, following the flat-field procedure recommended by Dexela). Five flat-field images were median-combined at each voltage to form the average flat-field image used for image correction at that voltage. For monochromatic imaging, where the spectrum of X-rays reflected by the mirror is essentially independent of tube voltage (i.e., there is no discernable beam-hardening), flat-field images were obtained using a tube voltage of 49 kVp, for maximum flux. As in the case of polychromatic imaging, five flat-field images were median-combined to form the average monochromatic flat-field image used for image correction.

The energy bandpass of the X-ray mirror when mounted in the test-stand is highly dependent on the tube's focal spot size. While the energy bandpass of X-rays reflected by the mirror is ∼1.3 keV FWHM as measured using the low-divergence pencil beam in the hard X-ray reflectometer described above (Fig. 4), the bandpass increases to ∼1.5 keV when using the 0.1 mm focal spot in the cone-beam geometry (Fig. 6) and to ∼4 keV when using the 0.3 mm focal spot (not shown in Fig. 6). In order to realize the most narrow energy bandpass possible when acquiring monochromatic images with the scanning X-ray mirror for the purposes of this study, the 0.1 mm focal spot was used in all cases. Furthermore, the same size focal spot was used for polychromatic image acquisition as well, to facilitate direct comparison. The maximum filament current that can be used with the 0.1 mm focal spot is 32 mA, however. Because of the reduced tube output when operated using the small focal spot, the detector was configured for operation in the "low-full-well" (i.e., high-gain) mode in order to minimize exposure times (at the expense of increased detector noise).

G. Image quality measurements

For each of the nine phantom assemblies, three images were acquired in succession (i.e., without moving the phantom) for each technique, i.e., for each combination of tube voltage and mA s investigated for polychromatic images, and for each mA s value investigated (i.e., at 49 kVp tube voltage, in all but two cases, as explained below) for monochromatic images. Following the methodology described by Williams *et al.*,[25] for each set of three images, several regions of interest (ROIs) were used to compute contrast, signal-difference and noise. The ROIs used are illustrated in Fig. 7, which shows a typical pair of polychromatic and monochromatic images of a common phantom. Four square ROIs comprising 120 × 120 pixels were defined to include the glandular step (the ROIs labeled "G" in Fig. 7), the calcification step (the ROIs labeled "C"), and the corresponding reference ROIs (i.e., containing no embedded features) adjacent to these two steps (the ROIs labeled "G_{Ref}" and "C_{Ref}," respectively). The signal-difference for a given step is computed as the difference

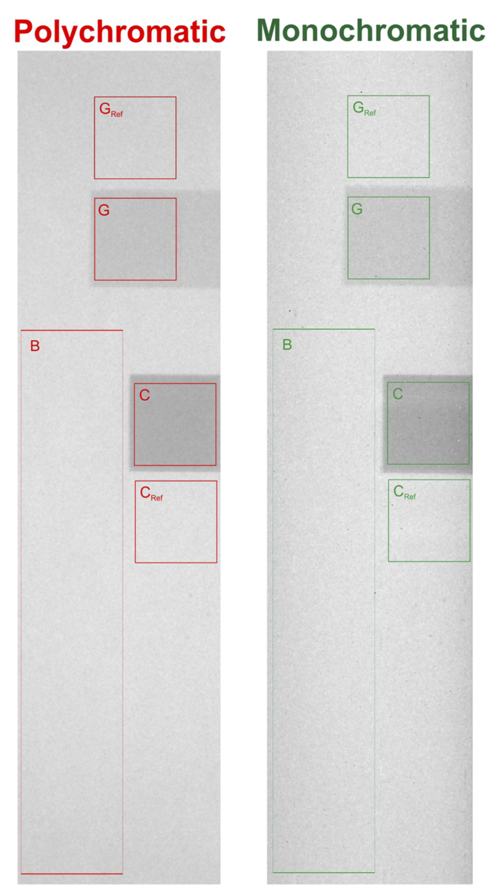

FIG. 7. Polychromatic (left) and monochromatic (right) images of a portion of the 7 cm-thick phantom having 30% glandular composition. Regions of Interest (ROIs) containing a 0.3 mm-thick calcification step (labeled "C") and a 10 mm-thick glandular step (labeled "G"), as well as reference and background ROIs (explained in the text), were used to compute image contrast and SDNR for both features.

between the average pixel value of the ROI containing the step and the average pixel value of the corresponding reference ROI. The contrast for a given step is computed as the signal-difference so computed divided by the average pixel value of the reference ROI. The flat-field procedure described in Sec. II F effectively removes large intensity variations due to the heel effect, and furthermore the reference regions used for signal and contrast computation were located at the same distance from the chest wall position as the corresponding step regions (i.e., the phantoms were oriented 90° relative to the orientation used in Ref. 25); consequently, signal de-trending was not performed. Statistical image noise was computed using a fifth, larger rectangular "background" ROI (labeled "B" in Fig. 7), comprising 150 × 800 pixels and containing no embedded features. The difference image computed by subtracting two of the three successively acquired images of the same phantom (i.e., all obtained using a common technique) was used to compute uncorrelated image noise: the root-mean-square uncorrelated noise is calculated as the standard deviation of the pixel values in the background region of the difference image divided by $\sqrt{2}$,

$$\text{Noise} = \text{Std. Dev.}\ (\text{ROI}_{\text{B,i}}(\text{x, y}) - \text{ROI}_{\text{B,j}}(\text{x, y}))/\sqrt{2}, \qquad (2)$$

where the indices i and j denote two different images of the same phantom. The SDNR is then computed as the signal-difference divided by the noise. Finally, for each phantom and imaging technique, a figure-of-merit (FOM) function was computed as

$$\text{FOM} = \text{SDNR}^2/\text{MGD}. \qquad (3)$$

With the acquisition of three images for each phantom and imaging technique, three independent values for contrast, SDNR and FOM were computed; the representative value of each of these three quantities was calculated as the mean of the three independently measured values.

For each of the nine breast phantoms, conventional polychromatic (i.e., W/Rh) images were obtained at tube voltages in the range 20–34 kVp, in 2 kVp steps, and for current-time products within the available 5–320 mA s range at each tube voltage, in order to identify the optimum (polychromatic) technique in each case. Pixel saturation limited the maximum current-time product used at each tube voltage, and the minimum current-time product considered was determined by the minimum required average pixel value for background regions, selected for this investigation to be 500 counts/pixel. The optimal polychromatic technique for each phantom was defined as that technique that gave the maximum FOM [Eq. (3)] for the glandular step.

Monochromatic images were obtained for each of the nine phantoms as well: the tube voltage was held at 49 kVp (in all but two cases, explained below) to minimize exposure time; the reflected X-ray spectrum is essentially independent of tube voltage, so maximum tube voltage can be used. The current-time product was varied systematically up to the point where the SDNR for the glandular step was equal to or greater than the SDNR for the same feature obtained using polychromatic radiation for the selected technique that produced the maximum FOM as just described; the monochromatic image having the same SDNR (to within +8/−5%) for the glandular step as obtained using polychromatic radiation was then selected for quantitative comparison with the corresponding polychromatic image. Due to the generator's maximum allowable exposure time of 10 s, for many monochromatic images it was necessary to acquire and combine multiple exposures to form

TABLE I. Technique, exposure, HVL (polychromatic only), DgN, MGD and IQ computed for a 0.3 mm-thick calcification step and a 10 mm-thick glandular step, for both polychromatic and monochromatic images, as a function of breast thickness and glandularity.

Gland (%)	Thickness (cm)	kVp	mA s	Exposure (mR)	HVL (mm Al)	DgN (mrad/R)	MGD (mGy)	0.3 mm calc. step Contrast	0.3 mm calc. step SDNR	0.3 mm calc. step FOM	10 mm gland. step Contrast	10 mm gland. step SDNR	10 mm gland. step FOM
						Polychromatic (W/Rh)							
30	3	22	40	47.5	0.454	328.0	0.156	0.349	24.6	3874	0.150	10.3	681
30	5	24	80	158.0	0.514	251.4	0.397	0.251	23.3	1365	0.092	8.2	172
30	7	26	100	274.4	0.545	200.0	0.549	0.213	15.8	457	0.070	4.9	43
50	3	24	32	59.2	0.514	348.8	0.206	0.289	26.8	3487	0.096	8.7	365
50	5	24	80	158.0	0.514	234.0	0.370	0.241	19.1	983	0.071	5.4	78
50	7	28	100	342.6	0.563	193.9	0.664	0.192	15.4	358	0.048	3.7	21
70	3	24	32	59.2	0.514	330.7	0.196	0.314	26.2	3507	0.043	3.5	63
70	5	28	50	160.1	0.563	243.9	0.391	0.241	19.6	982	0.021	1.7	7
70	7	28	80	274.1	0.563	178.4	0.489	0.214	12.3	309	0.018	1.0	2
						Monochromatic (~19 keV)							
30	3	49	320	22.2	N/A	425.9	0.094	0.309	25.8	7032	0.132	11.1	1299
30	5	49	640	47.3	N/A	283.5	0.134	0.265	18.3	2492	0.113	7.8	455
30	7	49	1280	101.3	N/A	204.9	0.207	0.227	12.2	720	0.097	5.2	131
50	3	49	420	29.1	N/A	399.0	0.116	0.291	25.2	5473	0.099	8.3	598
50	5	49	640	47.3	N/A	258.0	0.122	0.244	15.4	1923	0.085	5.4	240
50	7	49	1280	101.3	N/A	183.6	0.186	0.201	9.8	514	0.072	3.6	68
70	3	45	320	20.4	N/A	378.6	0.077	0.390	19.9	5153	0.071	3.7	176
70	5	45	320	21.8	N/A	239.9	0.052	0.254	10.6	2136	0.041	1.7	56
70	7	49	640	50.6	N/A	169.0	0.086	0.176	4.6	249	0.036	1.0	11

each of the three "final" images used for analysis in order to achieve the requisite SDNR. Furthermore, as a result of the tube being operated at maximum voltage, maximum current and maximum exposure time over the many weeks of time required to acquire the monochromatic images used in this investigation, the tube finally began to arc when operated at 49 kVp while imaging the final two phantoms investigated (7 cm thickness, 30% and 50% glandular fraction). Consequently, these phantoms were exposed using 45 kVp to avoid arcing.

For both polychromatic and monochromatic images, only a 325 pixel × 1320 pixel sub-region of the full image field was used for analysis, an area that includes the calcification step, the glandular step and the requisite background regions. While the full 16 × 22 cm^2 image field was illuminated in the case of polychromatic images, to minimize exposure time in the case of monochromatic images, the X-ray mirror was scanned only over an angular range of $\Delta\alpha = 2.25°$ (~2.6 × 22 cm^2 field size), which is slightly larger than the

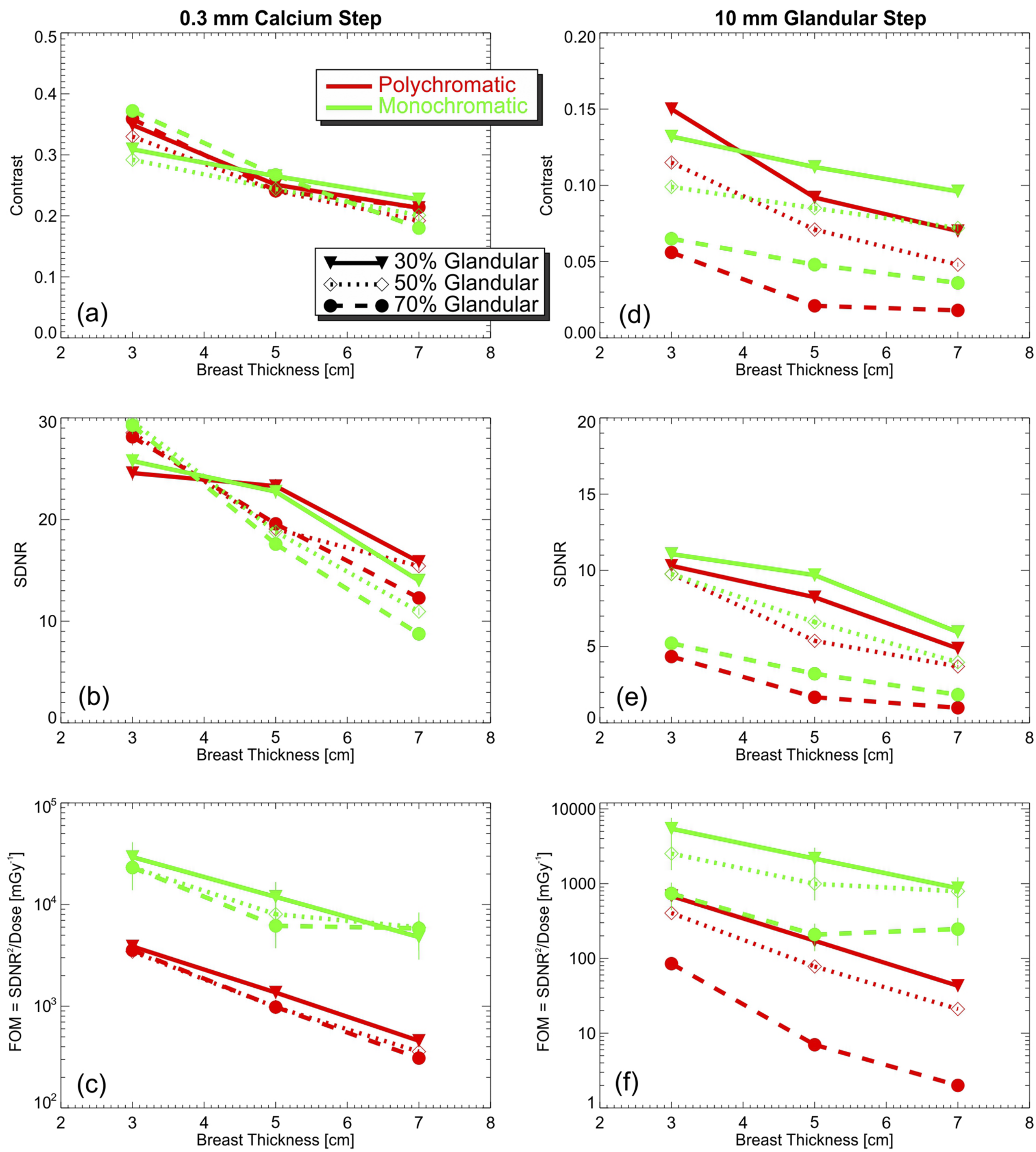

FIG. 8. Contrast, SDNR and FOM as a function of breast thickness and glandularity, measured for both polychromatic and monochromatic (19 keV) radiation. The image statistics computed for the 0.3 mm-thick calcification step are shown in (a)–(c), while those computed for the 10 mm-thick glandular step are shown in (d)–(f).

325-pixel-wide region used for image analysis. The reduction in scattering resulting from the smaller illuminated area in the monochromatic case, and its impact on IQ, is estimated to be relatively small, based on previous Monte Carlo studies:[29] for the particular imaging configuration used here, the reduction in the scatter-to-primary ratio is estimated to be less than 7%, and the resulting increase in contrast is estimated to be less than 3%.

III. RESULTS

Experimental results are shown in Table I and in Figs. 8–10. The contrast, SDNR and FOM computed for the calcification step are shown in Figs. 8(a)–8(c) as a function of breast thickness and glandularity, for both polychromatic and monochromatic exposures; similarly, Figs. 8(d)–8(f) show the contrast, SDNR and FOM for the glandular step. Shown in Fig. 9 is the relative dose, i.e., the MGD, obtained with monochromatic radiation relative to the MGD obtained with polychromatic radiation, as a function of breast thickness and glandularity. Finally, shown in Fig. 10 is the relative exposure time required for monochromatic image acquisition (i.e., using a single mirror scanned over an angular range of $\Delta\alpha = 2.25°$) as compared to polychromatic image acquisition, also as a function of breast thickness and glandularity.

As indicated in Table I, the optimal tube voltage for polychromatic imaging varied from 22 kVp to 28 kVp, depending on breast thickness and glandularity, with higher voltages required for thicker, denser breasts, as expected. Only a slight variation in maximum FOM with kVp was found, commensurate with the findings for W/Rh of Williams *et al.*[25] For most phantoms, comparable FOM values could be obtained using two or more different techniques.

Table I and Fig. 8 show that, while the monochromatic images selected for further analysis indeed have SDNR values for the glandular step [Fig. 8(e)] that are close to the corresponding SDNR values obtained using polychromatic radiation, the glandular step contrast values [Fig. 8(d)] for monochromatic radiation are substantially higher—by a factor of ∼2 for the 5- and 7 cm-thick 70% glandular phantoms—than those obtained using polychromatic radiation, in all cases but the 3 cm-thick 30% glandular phantom, where the monochromatic contrast is 88% of the polychromatic contrast. It is also evident from Table I and Fig. 8(a) that monochromatic images have higher contrast for the calcification step in all but two cases (the 3 cm/30% and 7 cm/70% phantoms). However, the calcification step monochromatic SDNR values are lower than the polychromatic SDNR values in all but one case [Fig. 8(b)]: the monochromatic SDNR values range from 37% to 105% of the polychromatic SDNR values for this feature. (Monochromatic images having SDNR values closer to the polychromatic values were also obtained: they required longer exposures, and corresponding dose increases; the doses are nevertheless substantially lower than the polychromatic values in all cases.)

A reduction in MGD when using monochromatic radiation was observed for all breast thicknesses and glandularities, as illustrated in Fig. 9. The highest relative dose (0.606) was measured for the 3 cm/30% phantom, while the lowest relative dose (0.134) was measured for the 5 cm/70% phantom. The relative dose decreases with increasing glandularity for all breast thicknesses. The reduction in MGD is primarily (but not exclusively) responsible for the improved monochromatic FOM values shown in Figs. 8(c) and 8(f) for both types of features, observed in all cases except for the 7 cm/70% phantom. The relative FOM values (i.e., the ratio of the monochromatic to the polychromatic FOM values) range from 0.8 to 2.2 for the calcification feature, and from 1.6 to 8.1 for the glandular feature, depending on breast thickness and glandularity.

Finally, Fig. 10 shows that monochromatic exposure times are ∼6–13 times longer than polychromatic exposure times, albeit using the fan beam produced from a single multilayer

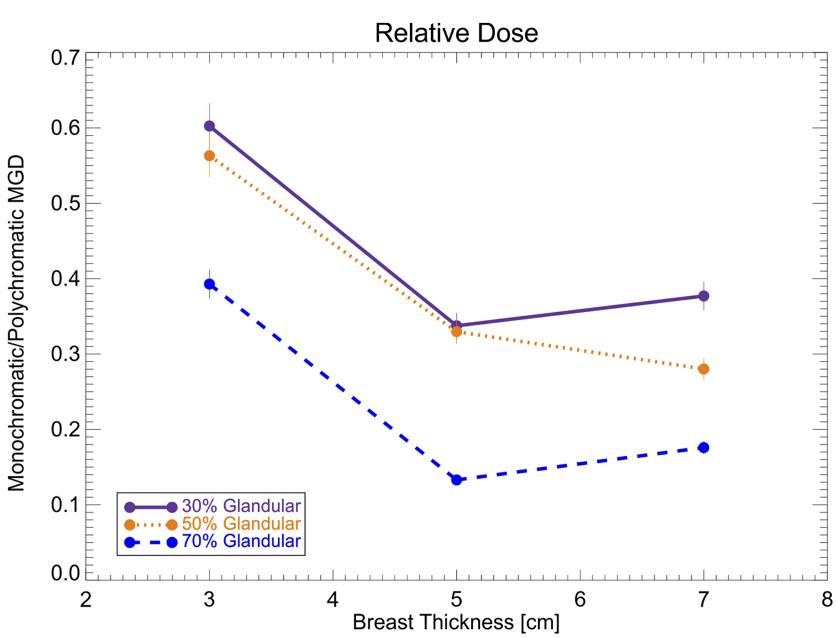

FIG. 9. Relative MGD of monochromatic (19 keV) radiation to polychromatic (W/Rh) radiation required for monochromatic images having SDNR values for the 10 mm-thick glandular step that are approximately equal to the corresponding SDNR obtained using polychromatic radiation.

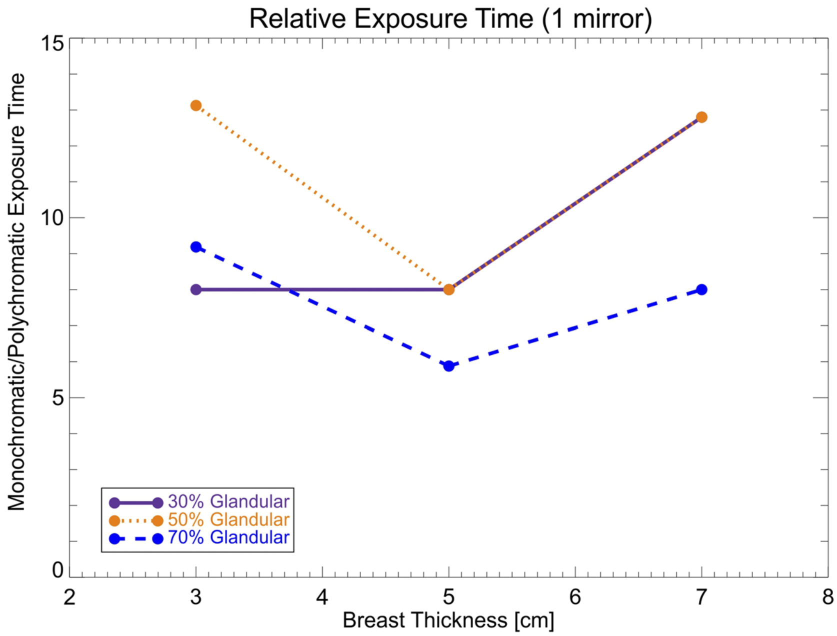

FIG. 10. Relative exposure time required for acquisition of monochromatic (19 keV) images, obtained using a single mirror scanned over an angular range of 2.25°, relative to the exposure time required for polychromatic (W/Rh) images.

mirror scanned over a 2.25° angular field size. (Note that the exposure times used in Fig. 10 for the 3 and 5 cm/70% phantoms, which were exposed at 45 kVp, have been scaled to reflect the somewhat smaller exposure times that can be realized when using 49 kVp tube voltage.) Possible paths to even better SDNR and contrast and, crucially, potential strategies to realize acceptably short exposure times and large image fields, as required for clinical application, are discussed in Sec. IV.

Note that, in the case of monochromatic exposures, it was found from examination of the X-ray spectra over time that the central energy of the reflected fan beam drifts toward higher energies as the tube temperature increases: while the mirror was aligned so as to produce a central X-ray energy of ~18.5 keV with a cold tube, the central energy of the reflected beam could drift as high as ~19.5 keV after 1-2 h of continual use, when the tube typically reached about 40% of its maximum heat capacity, at which point the tube was allowed to cool before further images were acquired. This energy drift is almost certainly due to thermal effects within the tube: a change in the focal spot position as the anode is heated from use can result in a change in the incidence angle of X-rays relative to the mirror surface, thereby shifting the energy of reflected X-rays that satisfy the Bragg condition. But whatever the cause, as a consequence of the observed drift in beam energy with tube temperature, the central X-ray energy used to produce a given monochromatic phantom image is uncertain to within ±0.5 keV. Furthermore, the observed energy drift results in uncorrected systematic errors in the monochromatic dose measurements (due to the variation in DgN with energy for monochromatic radiation); the experimental uncertainty in monochromatic MGD values due to energy drift is estimated to be ±5%.

IV. DISCUSSION

The imaging test-stand (Fig. 1) was designed to demonstrate the feasibility of using a scanning multilayer X-ray mirror system for large-area monochromatic imaging in a clinically practical configuration, and to facilitate direct comparison of IQ and dose between monochromatic and polychromatic radiation using a common X-ray tube, imaging detector and breast phantoms. The test-stand was not intended to produce optimized polychromatic images commensurate with those that can be obtained using commercial DM systems. The test-stand uses no anti-scatter grid, and systematic reduction of X-rays scattered by the tube mounting hardware, the collimator, the alignment system and the mirror scanning system was not performed. In comparison with the commercial W/Rh system used by Williams *et al.*[25] (Siemens Mammomat Novation DR), the polychromatic images produced using the test-stand in fact show somewhat lower image contrast and SDNR values, e.g., contrast of 0.28 vs. 0.24 and SDNR of 20 vs. 19.1, in the case of the calcification step embedded in a 5 cm-thick 50% glandular phantom. The slightly lower contrast and SDNR values obtained with the test-stand may be the result of increased scatter relative to the commercial system, to detector and image processing differences, and/or to differences in the X-ray spectra used in the two systems, despite the common W/Rh anode/filter combination. In addition, the test-stand was operated using the 0.1 mm focal spot and the detector operated in the high-gain mode for all cases, which results in dose values for polychromatic radiation in the range of 0.16–0.66 mGy, depending on breast thickness and glandularity; these dose values are approximately 30% of the dose values reported by Williams *et al.* for images obtained using the commercial system. The reduced dose (and exposure) in the case of the test-stand polychromatic images may also be correlated with a systematic decrease in contrast and SDNR. In any case, the reduced dose itself is likely the primary reason why the polychromatic FOM values reported here are so much larger than those reported by Williams *et al.*

In spite of the deficiencies of the imaging test-stand just outlined, the relative comparison between polychromatic and monochromatic images reported here is nevertheless meaningful (albeit with the uncertainties in monochromatic scattering, dose and beam energy already discussed). Furthermore, the observed improvements in contrast and dose are commensurate with previously reported results using monochromatic radiation. For example, Yoon *et al.*[14] reported a dose reduction of 12× and a contrast increase of 1.85× (albeit computed using a somewhat different formalism than that used here), with monochromatic radiation produced using a multilayer mirror tuned near 21.5 keV, for the case of an accreditation phantom (4.2 cm thick and 50% glandular composition). In any case, the present results showing reduced dose and increased IQ in the case of monochromatic imaging, along with the "proof-of-concept" demonstration of a scanning X-ray mirror system utilizing a stationary mammography tube and a large-area imaging detector arranged in a conventional geometry, illustrate the benefits and feasibility of developing monochromatic X-ray imaging systems using multilayer X-ray mirrors.

In order to use a standard mammography tube with scanning X-ray mirrors for the construction of an affordable, clinically practical breast imaging system, acceptable stability and sufficiently short exposure times must be realized. It may be possible to minimize, or perhaps eliminate, the drift in energy over time observed in the fan beam reflected by the X-ray mirror, described above, by orienting the mirror-scanner rotation axis 90° relative to the orientation shown in Fig. 1 such that it is nearly parallel, rather than perpendicular, to the tube's axial direction. Because of the tube geometry, focal spot motion resulting from heating may occur largely in the vertical plane, along the tube's axial and radial directions; with the scan axis nearly parallel to the tube axis, therefore, there may be little or no change in incidence angle due to heat-driven focal spot motion, which is the suspected cause of the energy drift. This alternate mirror-tube geometry will also facilitate patient positioning without interference by the scanner, to avoid chest-wall missed tissue.

A "wedged-stack" optic, comprising multiple co-aligned X-ray mirrors,[30] can be used in the future to realize shorter exposure times and large image fields. The monochromatic exposure times reported above are ~6–13 times higher than polychromatic exposure times, and furthermore correspond to a field size that is ~6× smaller in one direction; even longer exposure times may be needed to achieve acceptable monochromatic SDNRs for calcifications. If the single X-ray mirror used for the present work were replaced with a wedged-stack of 8 co-aligned X-ray mirrors simultaneously illuminating the same ~2.6 cm field size, for example, monochromatic exposure times would be reduced by a factor of 8; if the single mirror were replaced with a stack of $6 \times 8 = 48$ mirrors, an image field six times large (~16×22 cm^2) could be exposed over the same time. Further decreases in exposure time may be realized by using the larger 0.3 mm focal spot. This focal spot produces a larger energy bandpass (~4 keV, as explained above), however, so the improvements in IQ and dose reported here will be diminished to some extent. If the diminished monochromatic performance is nevertheless found to be better than polychromatic performance, as expected, then the large focal spot may provide the additional reduction factor of 2-3 (or perhaps more) that is needed to achieve clinically acceptable exposure times for all breast thicknesses and glandularities. If not, it may be necessary to utilize higher-power (and more expensive) X-ray tubes in the future. It will be necessary as well to also investigate tube heat loading, focal spot blooming and tube lifetime in order to assess commercial viability.

Further investigations using the imaging test-stand with X-ray mirrors tuned to different X-ray energies may reveal that even higher contrast SDNR and FOM values and lower MGD values can be achieved for certain breast thicknesses and glandularities, relative to the values reported here that were all obtained using one mirror tuned to 19 ± 0.5 keV. Modeling suggests that there exists an optimum X-ray energy for a given breast thickness and glandularity;[5] an energy of 19 keV is therefore unlikely to prove optimal in all cases. Indeed, the lower glandular contrast observed for the 3 cm/30% phantom, and the non-linear variations in dose with breast thickness (Fig. 9), suggest that better performance may be obtained for certain phantoms using other X-ray energies. It also will be possible to construct multi-energy wedged-stack mirror arrays, i.e., multiple wedged-stack optics, with each optic tuned to a different energy: once optimal monochromatic energies are established as a function of breast thickness and glandularity, multi-energy mirror arrays will enable the system operator to pre-select the monochromatic beam energy that is optimally matched to breast size and glandularity for each patient.[19] Multi-energy wedged-stack optic arrays will also facilitate the development of other monochromatic imaging modalities, including DBT, CESM and others.

V. CONCLUSIONS

A prototype monochromatic X-ray imaging test-stand has been developed using a scanning multilayer X-ray mirror in conjunction with a standard W-anode mammography tube and a large-area imaging detector arranged in a configuration typically used for mammography. Through a preliminary DM study using tissue-equivalent breast phantoms, the monochromatic (~19 keV) dose is found to be substantially lower than the polychromatic dose for images having comparable SDNR values. The largest reductions in dose were observed for the densest breasts. Figure-of-merit values for monochromatic images are higher (in all but one case) than those measured for polychromatic images as well, for both glandular and calcification features. Additionally, glandular contrast values for monochromatic radiation are substantially higher, by up to a factor of 2, than those obtained using polychromatic radiation, in all but one case.

The proof-of-concept, scanning X-ray mirror imaging system demonstrated here, and the preliminary measurements of improved IQ and lower dose when using monochromatic X-rays, will facilitate the future development of monochromatic DM, DBT and CESM systems for breast imaging, and potentially imaging systems for other applications as well. These new monochromatic imaging modalities are also expected to have better IQ, lower dose and potentially other performance improvements as well, and may yield substantial clinical benefits, potentially including better identification of deadly vs. non-deadly cancers, and reductions in overdiagnosis and overtreatment. Future research using refined imaging system designs will aim to achieve acceptable operating stability, and exposure times that are sufficiently short for clinical use when using conventional X-ray tubes, so that the benefits of monochromatic breast imaging can be delivered to the public.

ACKNOWLEDGMENTS

The author is grateful to R. Malzbender of RPM Associates for development of critical software and electronics, to M. Gould of Zen Machine (Lyons, CO) for the development of a variety of custom mechanical components required for this investigation, and to M. Williams and J. Boone for helpful technical discussions. This research was sponsored, in part, by Grant Nos. 1R43CA116969-01 (SBIR Phase I) and 2R44CA116969-02 (SBIR Phase II) awarded by the National Cancer Institute.

[1]NCI-funded Breast Cancer Surveillance Consortium co-operative agreement, "Performance measures for 1,960,150 screening mammography examinations from 2002 to 2006 by age–based on BCSC data as of 2009," November 15, 2011, http://breastscreening.cancer.gov/data/performance/screening/2009/perf_age.html.
[2]D. B. Kopans, "Digital breast tomosynthesis from concept to clinical care," Am. J. Roentgenol. **202**, 299–308 (2014).
[3]S. Vedantham, A. Karellas, G. R. Vijayaraghavan, and D. Kopans, "Digital breast tomosynthesis: State of the art," Radiology **277**, 663–684 (2015).
[4]P. C. Johns and M. J. Yaffe, "X-ray characterization of normal and neoplastic breast tissues," Phys. Med. Biol. **32**, 675–695 (1987).
[5]R. Fahrig and M. J. Yaffe, "A model for optimization of spectral shape in digital mammography," Med. Phys. **21**, 1463–1471 (1994).
[6]M. Biegata, T. Jakubowska, and K. Markowska, "Effect of anode/filter combination on average glandular dose in mammography," J. Med. Phys. **40**, 45–51 (2015).
[7]J. T. Bushberg, J. A. Siebert, E. M. Leidholdt, Jr., and J. M. Boone, in *The Essential Physics of Medical Imaging*, 2nd ed. (Lippincott Williams & Wilkins, Philadelphia, PA, 2002), Chap. 3.
[8]J. M. Boone and J. A. Seibert, "A comparison of mono- and poly-energetic x-ray beam performance for radiographic and fluoroscopic imaging," Med. Phys. **21**, 1853–1863 (1994).
[9]E. Burrattini, M. Gambaccini, M. Marziani, O. Rimondi, P. L. Indovina, M. Pocek, G. Simonetti, M. Benassi, C. Tirelli, and R. Passariello, "X-ray mammography with synchrotron radiation," Rev. Sci. Instrum. **63**, 638–640 (1992).
[10]K. Achterhold, M. Bech, S. Schleede, G. Potdevin, R. Ruth, R. Loewen, and F. Pfeiffer, "Monochromatic computed tomography with a compact laser-driven x-ray source," Sci. Rep. **3**, 1–14 (2013).
[11]E. Castelli, M. Tonutti, F. Arfelli, R. Longo, E. Quaia, L. Rigon, D. Sanabor, F. Zanconati, D. Dreossi, A. Abrami, E. Quai, P. Bregant, K. Casarin, V. Chenda, R. H. Menk, T. Rokvic, A. Vascotto, G. Tromba, and M. A. Cova, "Mammography with synchrotron radiation: First clinical experience with phase-detection technique," Radiolology **259**, 684–694 (2011).
[12]A. Bingölbali and C. A. MacDonald, "Curved crystal x-ray optics for monochromatic imaging with a clinical source," Med. Phys. **36**, 1176–1183 (2009).
[13]F. R. Sugiro, D. Li, and C. A. MacDonald, "Beam collimation with polycapillary x-ray optics for high contrast high resolution monochromatic imaging," Med. Phys. **31**, 3288–3297 (2004).
[14]K. H. Yoon, Y. M. Kwon, B.-J. Choi, H. H. Son, C. W. Ryu, K. S. Chon, S. H. Park, and S. K. Juhng, "Monochromatic x-rays for low-dose digital mammography," Invest. Radiol. **47**, 683–687 (2012).
[15]J. M. Lewin, P. Isaacs, V. Vance, and F. J. Larke, "Dual-energy contrast-enhanced digital subtraction mammography: Feasibility," Radiology **229**, 261–268 (2003).
[16]J. Folkman, K. Watson, and D. Hanahan, "Induction of angiogenesis during the transition from hyperplasia to neoplasia," Nature **339**, 58–61 (1989).
[17]M. Matsumoto, A. Yamamoto, I. Honda, A. Taniguchi, and H. Kanamori, "Direct measurement of mammographic x-ray spectra using a CdZnTe detector," Med. Phys. **27**, 1490–1502 (2000).
[18]D. L. Windt, S. Donguy, C. J. Hailey, J. Koglin, V. Honkimaki, E. Ziegler, F. E. Christensen, C. M. H. Chen, F. A. Harrison, and W. W. Craig, "W/SiC x-ray multilayers optimized for use above 100 keV," App. Opt. **42**, 2415–2421 (2003).
[19]D. L. Windt, "Mirror mounting, alignment, and scanning mechanism and scanning method for radiographic x-ray imaging, and x-ray imaging device having same," U.S. patent 7,978,822 (12 July 2011).
[20]D. L. Windt, "Optical alignment system and alignment method for radiographic x-ray imaging," U.S. patent 7,794,144 (14 September 2010).
[21]D. L. Windt and W. K. Waskiewicz, "Multilayer facilities for EUV lithography," J. Vac. Sci. Technol., B: Microelectron. Nanometer Struct.–Process., Meas., Phenom. **12**, 3826–3832 (1994).
[22]H. L. Marshall, N. S. Schulz, D. L. Windt, E. M. Gullikson, M. Craft, E. Blake, and C. Ross, "The use of laterally graded multilayer mirrors for soft x-ray polarimetry," Proc. SPIE **9603**, 960319 (2015).
[23]D. L. Windt, "Laboratory-based x-ray reflectometer for multilayer characterization in the 15–150 keV energy band," Rev. Sci. Instrum. **86**, 043107 (2015).
[24]D. L. Windt, "IMD—Software for modeling the optical properties of multilayer films," Comput. Phys. **12**, 360–370 (1998).
[25]M. B. Williams, P. Raghunathan, M. J. More, J. A. Seibert, A. Kwan, J. Y. Lo, E. Samei, N. T. Ranger, L. L. Fajardo, A. McGruder, S. M. McGruder, A. D. A. Maidment, M. J. Yaffe, A. Bloomquist, and G. E. Mawdsley, "Optimization of exposure parameters in full field digital mammography," Med. Phys. **35**, 2414–2423 (2008).
[26]J. M. Boone, "Glandular breast dose for monoenergetic and high-energy x-ray beams: Monte Carlo assessment," Radiology **213**, 23–37 (1999).
[27]J. M. Boone, "Normalized glandular dose (DgN) coefficients for arbitrary x-ray spectra in mammography: Computer-fit values of Monte Carlo derived data," Med. Phys. **29**, 869–875 (2002).
[28]A. L. C. Kwan, J. A. Seibert, and J. M. Boone, "An improved method for flat-field correction of flat panel x-ray detector," Med. Phys. **33**, 391–393 (2006).
[29]D. R. Dance and G. J. Day, "The computation of scatter in mammography by Monte Carlo methods," Phys. Med. Biol. **29**, 237–247 (1984).
[30]H. W. Schnopper, S. Romaine, and A. Krol, "X-ray monochromator for divergent beam radiography using conventional and laser produced x-ray sources," Proc. SPIE **4502**, 19–29 (2001).